Nanoscale

Accepted Manuscript

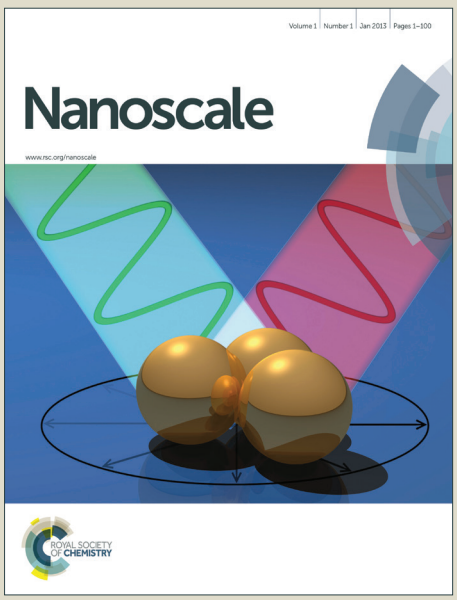

ROYAL SOCIETY OF CHEMISTRY

www.rsc.org/nanoscale

ARTICLE TYPE www. rsc.org/xxxxxx | XXXXXXXX

Efficient simulations of the aqueous bio-interface of graphitic nanostructures with a polarisable model†

Zak E. Hughes,*[a] Susana M. Tomásio[b] and Tiffany R. Walsh[a]

Received Xth XXXXXXXXXX 20XX, Accepted Xth XXXXXXXXX 20XX
First published on the web Xth XXXXXXXXXX 200X
DOI: 10.1039/b000000x

To fully harness the enormous potential offered by interfaces between graphitic nanostructures and biomolecules, detailed connections between adsorbed conformations and adsorption behaviour are needed. To elucidate these links, a key approach, in partnership with experimental techniques, is molecular simulation. For this, a force-field (FF) that can appropriately capture the relevant physics and chemistry of these complex bio-interfaces, while allowing extensive conformational sampling, and also supporting inter-operability with known biological FFs, is a pivotal requirement. Here, we present and apply such a force-field, GRAPPA, designed to work with the CHARMM FF. GRAPPA is an efficiently implemented polarisable force-field, informed by extensive plane-wave DFT calculations using the revPBE-vdW-DF functional. GRAPPA adequately recovers the spatial and orientational structuring of the aqueous interface of graphene and carbon nanotubes, compared with more sophisticated approaches. We apply GRAPPA to determine the free energy of adsorption for a range of amino acids, identifying Trp, Tyr and Arg to have the strongest binding affinity and Asp to be a weak binder. The GRAPPA FF can be readily incorporated into mainstream simulation packages, and will enable large-scale polarisable biointerfacial simulations at graphitic interfaces, that will aid the development of biomolecule-mediated, solution-based graphene processing and self-assembly strategies.

Introduction

Graphitic-nanostuctures, particularly graphene and carbon-nanotubes (CNTs), are promising candidates for wide-ranging applications, *e.g.* in biomedical applications,[1,2] biological imaging,[3] desalination[4] and biochemical sensors.[5–7] In particular, prediction and control of physico-chemical properties at the interface between biomolecules and graphene, in an aqueous environment, is pivotal to realising the full potential of such applications. Additionally, advances in electronic applications, where the doping behaviour of graphene can be modulated via the non-covalent adsorption of peptides, could be progressed via a deeper understanding of the structure/property relationships of this bio-interface[8,9]. Furthermore, development of non-biological graphene-based applications, such as in energy, which could profit from solution-based, biomolecule-mediated processing and self-organisation strategies, could also stand to benefit from predictable control of the aqueous bio-graphitic interface at the molecular level. Despite the prospect of these considerable gains, realisation of such predictable control over the structures of, and thus the properties delivered by, graphitic bio-interfaces is currently a challenging task. In partnership with experimental characterisation, molecular simulation offers a potential route to elucidating the molecular-level details needed to enable the design of next-generation biomolecules that possess such predictable bio-interfacial properties.

The adsorption of identified and/or selected graphitic-binding peptides at aqueous graphitic interfaces has been investigated experimentally,[9–18] with the identification of peptide sequences found to selectively bind to either the basal plane, or edges, of graphene flakes,[16,18], and to selectively bind to CNTs over planar graphite.[10] Direct observations of binding affinities (in terms of adsorption constants) for

† Electronic Supplementary Information (ESI) available: Details of the testing of four different DFT functionals; the adsorption energies and separation distances for the full set of analogue molecules; details of the adsorption energies of the phenyl species on the graphene surface at different adsorption sites; snapshots of the set-ups of the three different water-graphene simulations; plane-wave DFT minimum energy configurations of the full set of analogue molecules; details of the development and parametrisation of the GRAPPA FF; details of the parameters and setup used for the AMEOBAPRO simulations; the probability distribution of the O-H bond vectors of water molecules at the graphene interface; details of the simulation times for the (14×0) CNT systems using the different FFs; details of tests performed to determine the contribution of polarisability to binding energies; the RMSD between the reference values and plane-wave DFT values of different groups of molecules; 2D density maps of water on the graphene interface; density and hydrogen bond profiles for the simulations of water inside CNTs; 2D density maps of water inside the CNTs; plots of the collective variable against time for the meta-dynamics simulations; probability distributions of the angle between the plane of the aromatic rings and the graphene surface; the probability distribution of distance of the methyl carbon from the graphene surface for Ala. See DOI: 10.1039/b000000x/

[a] *Institute for Frontier Materials, Deakin University, Geelong, Australia. Fax: +61 (0)3 5227 1103; Tel: +61 (0)3 5247 9160; E-mail: zhughes@deakin.edu.au*
[b] *Department of Chemistry and Centre for Scientific Computing, University of Warwick, Coventry, CV4 7AL, U.K.*

these graphitic bio-interfaces have not yet been reported; nor has direct determination of the structure(s) of these peptide sequences when adsorbed at the aqueous graphitic interface. While direct structure observations of the dried peptide/graphitic interface have been reported, *e.g.* see Ref[19], it is currently not well understood how the results from the drying process differ from the interfacial peptide conformations in *solution*. Reports of indirect observation of peptide conformation changes upon adsorption at the aqueous graphitic interface, *e.g.* via circular dichroism (CD) spectroscopy are more commonplace–see *e.g.* Refs[8,20,21]. However, it is the combination of the peptide binding affinities, and their corresponding structures that, when correlated[22], can facilitate clear elucidation of the interplay thought to exist between peptide sequence, its adsorbed structure, and the resulting binding behaviour.[23,24]

Such elucidation can be guided via molecular simulations. In the absence of definitive experimental amino acid (AA) adsorption data, the adsorption of AAs at the aqueous graphitic interface have been investigated computationally.[25,26] Two recent theoretical studies reported calculations of the adsorption enthalpies of the different amino acids on graphene surfaces under aqueous conditions,[25,26] however, in both cases the force-fields (FFs) used (TEAM[26] and AMBER ff99SB[25]), modelled the graphene sheet as non-polarisable, meaning they may not fully capture the graphene-water/biomolecule interaction. In graphitic-nanostuctures, polarisability is likely to play an influential role (see below), especially given the number of AAs that carry an overall charge at a pH of 7. In addition, neither FF was tailored specifically for modelling aqueous biomolecular-graphitic interfaces.

Understanding the adsorption behaviour at the level of the AAs can provide a useful benchmark for interpreting both simulation and experimental data relating to *peptide* adsorption. However, due to the interplay between peptide sequence, structure and binding, the connections between amino acid adsorption and *residue* adsorption are not always clear. In this regard, simulations of peptide adsorption are necessary. The adsorption of graphitic-binding peptides at aqueous graphitic interfaces have been previously investigated computationally.[9,11,16,17,23,25–32] By elucidating the behaviour of peptides on graphitic-nanostructures, molecular simulation can aid the development of new peptide species that show controllable and predictable binding strengths and structures. Moreover, the spatial and orientational structuring of the solvent is thought to play an integral role in the adsorption behaviour of peptides at inorganic interfaces[24,33], and thus any reasonable graphitic/water force-field must be able to capture this structuring adequately. FF based simulations of the interface between liquid water and graphene/graphite[34–42] — see also Ref[43] and references therein—and, carbon-nanotubes (CNTs) with water—see Ref[44] and references therein—have been reported previously some detail. While there is general agreement between the simulations in places (*e.g.* the position of the peaks in the water density profile) other characteristics are less settled. One considerable point of disagreement is the contact angle of water droplets on graphite; see Ref[41] and references therein for a detailed commentary on these studies.

One factor many (but not all) of these past simulations (of water, AAs, and peptides at graphitic interfaces) have in common is the use of a force-field that describes the interface between the graphitic surface and the adsorbates (including liquid water) solely in terms of van der Waals (vdW) interactions—in other words, neglecting polarisation effects. A number of previous reports have assessed the contribution of explicit polarisation in the FFs used to model the interfaces of graphitic-nanostructures with either peptides or water.[23,29,39,45–49] Zhao and Johnson derived a FF that incorporated polarisability via atomic quadrupoles on graphite and water,[46] reporting that the polarisation contribution was significant for polar fluids such as water. The extension of the polarisable AMOEBAPRO force-field to graphitic nanostructures[23] also identified polarisation as an essential contribution to the interaction energy of charged species. More recently, a study by Ho and Striolo[39] found that including an explicit description of polarisablity in a FF enhanced the number of water molecules with an O-H bond orientated towards the surface. In determining the adsorption energies of ions with a graphene surface *in vacuo*, Schyman and Jorgensen reported that the inclusion of polarisation was essential to get good agreement with the adsoption energies calculated using first principles methods.[49]

Therefore, one of the chief challenges inherent to simulation of aqueous graphitic bio-interfaces is the identification of a FF that can describe both the graphitic-water and graphitic-peptide interactions appropriately, while at the same time be sufficiently computationally inexpensive to permit the simulation over appropriate time- and length-scales, in addition to being compatible with commonly-used biomolecule FFs. In this sense, the non-polarisable interfacial force-fields in common usage may neglect important contributions, while on the other hand, the currently available polarisable force-fields either suffer from much greater computational expense, and/or are not harmonised with widely-used biomolecule force-fields, such as AMBER or CHARMM. Here, we construct an economical polarisable interfacial force-field, designed to work in partnership with the CHARMM FF, informed by *in vacuo* first-principles (FP) calculations.

Recent reports of quantum-chemistry-based investigations of the non-covalent interaction of various small molecules, especially water, with graphtitic carbon-nanostuctures are extensive .[49–66] Such weak interactions can be challenging to capture via electronic structure theory. In many of these studies the graphene sheet was approximated by arene rings

(*e.g.* benzene, coronene); however, the delocalised states at the surface will not be captured, and edge effects may be present. An alternative to post Hartree-Fock approaches is to use periodic density functional theory (DFT) to model infinite, planar graphene surfaces. However, traditional DFT functionals based on the generalised gradient approximation (GGA) cannot recover the dispersion contribution to the interaction energy, at mid- to long-range separations, limiting their applicability.[67] More recently, new functionals, involving nonlocal contributions to the correlation functional,[68,69] such as the vdW-DF family of functionals, have improved the performance of DFT in this regard. Such functionals have shown promising results in determining the weak interactions of small molecules on metal surfaces[70–73] as well as on graphene.[61,63] Previously, we have successfully used revPBE-vdW-DF to calculate the non-covalent adsorption of small organic molecules (relevant to peptides) onto gold and silver surfaces, for the parametrisation of the classical AgP/GolP-CHARMM force-fields.[71,73,74] In these FFs, the metal atoms were fixed in place, while a rigid-rod dipole approach is used to efficiently capture the polarisability of such systems.[75] While still only recently developed, the initial results from simulations using these FFs appear promising.[22,73] Thus, we have taken a similar approach here in developing our graphitic/water/peptide FF, GRAPPA.

The validation of any FF is a long term process, necessitating use of the FF to model many different systems against which relevant experimental data are available. Unfortunately, for the aqueous graphitic bio-interface, there is a lack of direct experimental data for such purposes. However, as an initial validation procedure, the structure of the interface of graphitic systems with water was investigated using GRAPPA. In this instance there are FP simulation data available for both graphene/water and CNT/water interfaces.[76–78] For comparison, we have modelled these two types of systems using molecular dynamics (MD) simulations and the GRAPPA FF, employing set-ups closely matched to these FP simulations. In addition, in light of the known drawbacks of FP simulations for these systems, we also tested GRAPPA against a more expensive polarisable FF, by conducting validation simulations using the AMOEBAPRO FF.[27,79–81] Following this, we then applied GRAPPA in meta-dynamics simulations,[82] to calculate the free energy of adsorption of a range of representative AAs at the aqueous graphene interface, and predict their likely conformations when adsorbed at this interface. In summary, the performance of GRAPPA, alongside its efficient implementation in a mainstream MD simulation package in partnership with the CHARMM FF, will enable large-scale simulations of aqueous graphitic bio-interface while incorporating polarisation effects.

Methods

DFT calculations

All DFT calculations were performed using the Quantum Espresso code (version 5.0.1),[83] with ultrasoft pseudopotentials[84] generated from scalar relativistic calculations. Initial tests compared the results obtained using four different exchange-correlation functionals: revPBE-vdW-DF,[68] vdW-DF2,[85,86] optB88-vdW-DF[87] and vdW-DF-C09.[88] On the basis of these data, we identifed the revPBE-vdW-DF functional as the most appropriate to calculate the adsorption energies/separation distances for the full set of 24 molecules (summarised in Table S1, ESI†) that were used as amino acid analogues.

The binding energies of the molecules were determined from

$$E_{\text{ads}} = E_{\text{Gra-mol}} - E_{\text{Gra}} - E_{\text{mol}} \quad (1)$$

where $E_{\text{Gra-mol}}$, E_{Gra} and E_{mol} are the potential energies of: the system with the molecule adsorbed to the graphene surface, the graphene sheet, and, the molecule in vacuum, respectively. All systems were geometry-optimised, prior to single-point calculations, used to determine the final energy of the systems.

Plane-wave DFT calculations were carried out on a 4×4 supercell, except for hexane, ethyl acetate, indole and diethyl sulphide where a 6×6 supercell was used. The experimentally determined C-C bond length of 1.42 Å was used to construct the supercells. The cut-offs for the plane-wave kinetic energies and electron densities were 40 and 340 Ry, respectively.

All systems had periodic boundary conditions applied in all three dimensions, and were constructed such that along the z-axis the molecule was separated from the periodic image of the graphene sheet by a distance of $\sim$16 Å during the geometry optimisation and $\sim$20 Å for the single point calculations. A k-point mesh of $4 \times 4 \times 1$ was used for the geometry optimisations and an $8 \times 8 \times 1$ mesh used for the single-point calculations. A force convergence criterion of 0.001 Ry/Å was applied for the geometry optimisations and the forces were checked during the single point calculations to ensure this threshold was not exceeded.

The initial configurations of the molecules were either taken from previous theoretical studies,[56,64] and/or used the optimised configuration of a similar molecule as a starting point. All molecules were optimised from multiple initial configurations.

In vacuo force-field parameter fitting

As found in related FFs such as GolP-CHARMM and AgP-CHARMM[71,73], each substrate carbon atom in GRAPPA possessed a rigid-rod dipole. A full description of the details of

the GRAPPA FF is given in the ESI†. The CHARMM22* FF[89,90] was used to model the amino acid analogue molecules. To determine how well GRAPPA reproduced the E_{ads} resulting from our DFT calculations, the full set of the twenty four analogue molecules was divided into a fitting set and a validation set. The parameters for GRAPPA were fitted against the energies and geometries of the molecules in the fitting set, and the FF results for the validation set were then tested against our DFT findings. Each set contained species featuring different functional groups: alkanes, alkenes, oxygen-, nitrogen- and sulphur- containing species. In addition, where possible, the types of molecules were further distinguished (*i.e.* hydroxyl oxygen and carbonyl oxygen) and an example of each was placed in both sets. The full details of the *in vacuo* FF simulations are given in the ESI†. The FF gromacs files are available from the authors upon request.

Evaluation of Polarisation Effects

Here, we have carried out interaction energy calculations both with and without the graphene carbon polarisation contribution, to evaluate image-charge contributions in our systems. We considered co-adsorption of the capped amino acid Arg (with +1 charge on the side-chain) and a Cl^- ion adsorbed at the graphene surface *in vacuo*. We also considered co-adsorption of the capped amino acid Asp (with -1 charge on the side-chain) and a Na^+ ion adsorbed at the graphene surface *in vacuo*. We found that the polarisation contribution in both cases was substantial, *e.g.* amounting to $\sim$65 kJ mol^{-1} for Arg, which was $\sim$40 % of the total interaction energy calculated using polarization. A similar result was found for adsorption of Asp. Full details of these calculations are given in the ESI† Section 'Polarisation Contribution Tests'.

GRAPPA MD simulations

The MD simulations of the water-graphene interfaces, the water within the carbon nanotubes and the adsorption of amino acids with the aqueous graphene interface were performed using GROMACS version 4.5.5.[91] The PLUMED plugin[92] was used to apply the well-tempered meta-dynamics approach[82] for the amino acid adsorption simulations. The CHARMM-modified version of the TIP3P[93,94] water model was used for the water molecules and the CHARMM22* FF parameters used for the amino acids[89,90]. For these simulations a time-step of 1 fs was used with the LJ non-bonded interactions switched off between 10.0 and 11.0 Å and a cut-off of 13.0 Å used for the PME summation.

The simulation of the graphene-water interface was tested using three different system setups shown in Figure S1. In System 1, two single layers of graphene, 49.19×42.60 Å, were separated by 48 Å of water (3166 molecules) and 32 Å of vacuum, thus ensuring that any water-water interaction through the graphene sheet is reduced to a minimum. In System 2, a single layer of graphene was solvated in a box of 3166 water molecules, with the cell dimensions measuring $49.19 \times 42.60 \times 48.2$ Å. In System 3, three layers of graphene are stacked on top of each other (in the ABA configuration) to model a graphite slab, and solvated in a box of 2918 water molecules ($44.27 \times 38.34 \times 61.00$ Å). For each system the length of the periodic cell along the z axis (*i.e.* the distance between the graphene sheets) was altered such that the density of water was equal to that obtained from a box of modified TIP3P water simulated at 300 K and 1 atm. Following this, production runs of 20 ns duration were performed in the Canonical (*NVT*) ensemble with the Nosé-Hoover thermostat[95] used to maintain the temperature at 300K.

For the simulations of water molecules within (14×0) and (19×0) CNTs, we followed the set-up from existing FP simulations. Nanotubes of length 51.112 Å were used. The (14×0) CNT contained 67 water molecules and the (19×0) CNT 130 water molecules. These systems were simulated for 20 ns at 300 K in the Canonical ensemble, with the temperature maintained via the Nosé-Hoover thermostat.

The adsorption free energy of six different AAs—Ala, Arg, Asp, Gly, HisA (the nonprotonated form of histidine), Phe, Trp and Tyr—at the aqueous graphene interface was also calculated. These AAs were chosen as they cover the range of different amino acid types (*i.e* positively charged, negatively charged, polar uncharged, apolar aliphatic and apolar aromatic). In addition, there is a lack of agreement in the literature regarding the relative ordering of the aromatic AA adsorption energies (in the absence of definitive experimental data). Therefore, we have calculated ΔG_{ads} for all four aromatic species. The L-chiral forms of the amino acids were modelled with the amino acids capped by acetyl and N-methyl groups at the N- and C-termini, respectively. The AAs were modelled according to their protonation state at pH 7 with either a Na^+ or Cl^- used as a counterion to ensure overall charge neutrality where necessary. Each system contained 2325 water molecules, between two graphene sheets 44.27×38.34 Å separated by 44 Å water and 36 Å of vacuum.

The free-energy of adsorption of the amino acids at the aqueous graphene interfaces was calculated using the well-tempered meta-dynamics approach[82]. All of these simulations were carried out in the Canonical (*NVT*) ensemble at a temperature of 300 K, using the simulation details as already specified. The bias was applied on the position of the centre of mass of each amino acid along the z-axis (*i.e.* the direction perpendicular to the graphene surface). Gaussians of 0.5 Å width were deposited every 1 ps for a total simulations time of 100 ns per AA, and the initial Gaussian height was set to 0.15 kJ mol^{-1}. A well-tempered meta-dynamics bias factor of 10 was used. The zero-point of the free-energy was calculated as the

Table 1 Adsorption energies, E_{ads}, and separation distances, d_{sep}, of the various analogue molecules and the graphene surface determined from both our DFT (revPBE-vdW-DF) calculations and the GRAPPA force-field.

Molecule	E_{ads} / kJ mol^{-1}			d_{sep} / Å			Set
	Ref.	DFT	GRAPPA	Ref.	DFT	GRAPPA	
Methane	-13.5[a]	-16.6	-13.3	3.31[a]	3.53	3.30	Fitting
Ethane	-20.8[a]	-23.7	-22.6	3.44[a]	3.69	3.47	Fitting
Hexane	-51.0[b]	-56.6	-53.6		3.78	3.51	Fitting
Benzene	-43.1[a], -48.2[c]	-46.9	-47.0	3.30[a]	3.59	3.32	Fitting
Toluene	-56.5[b]	-57.6	-55.7		3.60	3.33	Validation
Ethene	-20.2[a]	-22.6	-17.4	3.24[a]	3.52	3.35	-
Water	-13.5[a]	-13.2	-13.3	3.19[a]	3.51	3.20	Fitting
Ethanol	-30.5[b]	-29.9	-29.3		3.33	3.11	Validation
Acetone	-34.3[b]	-37.4	-33.1		3.28	3.03	Validation
Ammonia	-13.4[a]	-13.4	-15.7	3.31[a]	3.65	3.29	-

[a] DFT/CC calculation[56]; [b] Experimental[64]; [c] Experimental[96].

average free-energy at a distance greater than 15.0 Å from the surfaces. The uncertainty was determined from the difference between the final free-energy and the average free-energy over the last 5 ns of simulation.

AMEOBAPRO simulations

MD simulations of the aqueous graphite interface, and water molecules within a (14×0) CNT, were performed using an extension of the AMOEBAPRO[27,79–81] FF using the TINKER code.[97] The AMOEBAPRO FF describes electrostatics via the distributed multipole approximation,[98,99] up to and including quadrupoles, and by inclusion of atom-based polarisabilities. Therefore, the description of the aqueous interface using AMOEBAPRO should be of a high quality, allowing the performance of the more approximate, but significantly cheaper, GRAPPA FF to be evaluated. Full details of the AMEOBAPRO simulations are given in section "AMEOBAPRO Simulation Details" in the ESI†.

Results and discussion

Reference DFT calculations

To identify the most appropriate functional for determining the graphene adsorption energies (and distances/geometries) for our full set of adsorbate molecules, four different functionals were tested against a set of 13 molecules, for which reference data in the form of the results of coupled-cluster (DFT/CC) calculations[56] and/or experimental data[64,96] were available. The full results of these tests are detailed in the ESI†, in the section "Testing of the DFT Functionals", as well as in Tables S2-S3 and Figure S2. We ultimately found the revPBE-vdW-DF functional gave the lowest RMSD over the energies of the reference set. Thus we used the revPBE-vdW-DF functional in our subsequent calculations.

The adsorption energies, E_{ads}, and separation distances, d_{sep} with the revPBE-vdW-DF functional for those molecules which have a reference value are given in Table 1. E_{ads} and d_{sep} for the full set of analogue molecules are given in Table S1. The minimum energy configuration of each molecule is shown in Figures S3-5 in the ESI†.

In the case of water there are two low-energy configurations, which have either one or both H atoms pointed towards a carbon atom (denoted one-leg and two-leg, respectively), see Figure S3(a) and (b) in the ESI†. DFT/CC calculations of water on graphene[56,60] have shown the two-leg configuration to be lower in energy, which agrees with most studies of water on arene rings[53–55,57]. However, one study of water on dodecabenzocoronene (DBC) using the CCSD(T) level of theory (with cc-pVDZ and aug-cc-pVTZ basis sets for graphene and water, respectively) reported the one-leg configuration to be lower in energy.[62]

Our periodic DFT calculations on planar graphene give the adsorption energies for the one- and two-leg configurations as -13.4 and -13.2 kJ mol^{-1}, respectively. Such a small energy difference means that the question is not of direct importance to the present study where our aim is to enable simulations of the aqueous bio-interface with graphene and CNTs at ambient temperatures. The corresponding AMEOBAPRO adsorption energy of water on graphene was calculated here to be -14.3 kJ mol^{-1}, with the two-leg configuration of water found to be the lowest in energy.

The results for methane warrant further discussion, where most previous studies have calculated the most favourable adsorption site above the ring centre, with three hydrogen atoms directed towards the surface.[56,61,66] Our calculated adsorption energies for adsorption atop a C atom, and in the centre of a ring, are -16.4 and -16.6 kJ mol^{-1}, respectively. In a high level (MP2 and coupled-cluster theory) study of methane adsorption on arene ring systems, Smith *et al.* calculated the

Table 2 Parameters for the interaction of graphitic carbon atoms with other atomic species

Interaction	σ / Å	ε / kJ mol^{-1}
C(graphene)-C(graphene)	3.30	0.35
C(graphene)-O(water)	3.38	0.45
C(graphene)-O(hydroxyl)	3.30	0.55
C(graphene)-O(carbonyl/amide)	3.10	0.40
C(graphene)-N(Lys/terminal)	3.40	0.70
C(graphene)-S	3.50	0.85
C(graphene)-H(water)	2.70	0.24
C(graphene)-H(polar/thiol)	3.00	0.24

adsorption energy of methane on coronene as -11.9 kJ mol^{-1} and estimated the adsorption energy of methane on graphene as -14.6 kJ mol^{-1}.[66]

The aryl adsorbates were also considered in detail in our calculations. Discussion of the minimum energy configurations of the aryl species is given in the section "Minimum energy configurations of the aryl species" of the ESI†. The adsorption energies of the six different configurations of benzene, toluene and phenol are given in Table S4. Rajesh *et al.* calculated the binding energies for imidiazole, benzene, phenol and indole on graphene using a standard GGA functional as -20.3, -24.1, -29.9 and -40.5 kJ mol^{-1}, respectively.[28] The weak adsorption energies relative to the findings of the present study are due to the known limitations of the GGA functional but the trend is the same.

Derivation of GRAPPA parameters

Full details of the parametrisation of the GRAPPA FF are given in the ESI† section "Development of the GRAPPA force-field". The adsorption energies and separation distances of the different molecules on the graphene surface determined using GRAPPA are shown in Tables 1 and S1. The final values of the parameters for the the interaction of the graphene carbon atoms with the other atomic species are summarised in Table 2.

Graphene/CNT-aqueous interface

Previous MD studies investigating aqueous biomolecule–inorganic interfaces[22,24,33,71,73,74] indicate that the structuring of water at inorganic interfaces can play an vital role in determining biomolecule binding behaviours. Therefore it is essential that GRAPPA reproduce both the spatial *and* orientational distributions of water molecules at the interface.

The water density, hydrogen-bonding and orientational profiles of the graphene-aqueous interface, determined from simulations using both GRAPPA and AMEOBAPRO are shown in Figure 1. The results for the three system setups simulated

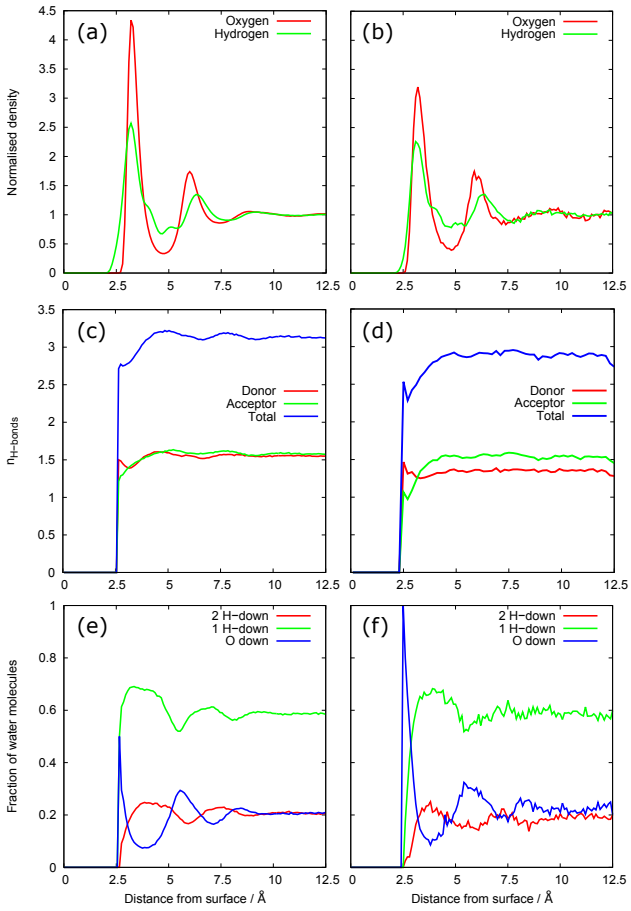

Fig. 1 Simulation data using GRAPPA (**a, c** and **e**) and AMOEBAPRO (**b, d** and **f**) of the graphene-water interface showing density profiles (**a**, **b**), number density hydrogen-bonding profiles (**c**, **d**) , and orientational profiles (**e**, **f**).

with the GRAPPA FF are almost identical; therefore, only the results for System 1 are shown. Our results can be compared against first-principles molecular dynamics (FPMD) simulations,[76–78] and the simulations of the SWM4-DP water model on a polarisable graphene FF.[39] Overall, GRAPPA captures of the main features of the graphene-aqueous interface; the position of the first and second peaks in the oxygen, and the hydrogen density profiles, agree well with both the AMEOBAPRO results and the FPMD simulations. Unlike the FPMD simulations, neither of the FFs used in this study supported a small shoulder to the hydrogen density profile at a separation distance of less than 2.5 Å, although both FFs featured a non-zero H density at this distance. The H-bond profiles also agree well with the FPMD simulations, showing a peak in the H-bond donor profile at the graphene surface. In the simulations of the interface performed using AMEOBAPRO there is an increased propensity for water molecules very close to the sur-

face to be oriented with the oxygen atom pointing down, but the position of the peaks and the general shape of the orientation profiles of the two FFs also agree well.

The probability distribution of the angle between the O-H bond vector and the normal of the graphene plane calculated for the water molecules in the first water layer ($r \leq 5.0$ Å) is shown in Figure S6. In summary the two FFs agree very well with each other and are in general agreement with the FPMD simulations. A more detailed discussion is given the the ESI† section "O-H bond vector probability distribution function".

The FPMD simulations of Cicero *et al.*[76] identified that the oxygen atoms of the water molecules in the first layer were found to be preferentially distributed above the centre of the rings while the deuterium atoms (the simulation was performed using D_2O) were preferentially distributed above the C-C bonds. The 2D density maps of oxygen atoms in first layer of water molecules in the GRAPPA simulations are shown in Figure S7(a) in the ESI†. In agreement with the FPMD simulations the oxygen atoms have a preference for the centre of the ring, however, the density map of the hydrogen atoms (Figure S7(b)) was effectively isotropic.

The mass density profiles and the hydrogen bonding profiles of the water molecules inside the carbon nanotubes are shown in Figure S8. There is good agreement between the AMEOBAPRO and GRAPPA FFs. Both FFs reproduce the main features of the density profiles reported in the FPMD study.[76] However, there were few differences; for the (14×0) CNT, Cicero *et al.* found the water density at the centre of the nantoube to be close to zero, while in the case of the (19×0) CNT, the height of the central peak was found to be approximately equal to those at the edge of the CNT. In all three sets of simulations (FPMD, AMEOBAPRO and GRAPPA) the hydrogen atoms are closer to the surface of the nanotube than the oxygen atoms. In addition, the FFs reproduces the peak in H-bond donors at the surfaces of both CNTs, and GRAPPA also reproduces the peak in total H-bonds at the surface of the (19×0) CNT. The 2D density maps of the oxygen and hydrogen atoms are shown in Figure S9 in the ESI†. These confirm that for the (14×0) CNT the density of water molecules at the centre of the CNT is zero, while in the case of the (19×0) CNT water molecules are present at the centre of the CNT.

We also used this system to make comparisons in the simulation timings between the AMOEBAPRO FF, the GRAPPA FF, and the unpolarised version of this FF (where we have removed the dipoles), denoted here as C22*. Full details of our timing runs are provided in the ESI† section "(14x10) CNT Simulation Timing Data". We found AMOEBAPRO was ∼1.5 *orders of magnitude* slower than GRAPPA. In stark contrast with this huge disparity in computation times between AMOEBAPRO and GRAPPA, only a relatively modest factor of 2 speed-up was seen for the unpolarised C22* compared with GRAPPA. GRAPPA, which appears to deliver results

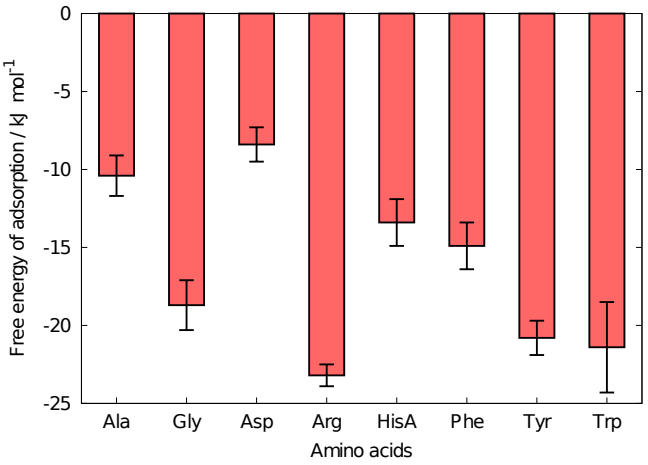

Fig. 2 The free energies of adsorption for the eight amino acids considered.

comparable with AMOEBAPRO, therefore represents a reasonable and economically viable approach to describing the polarisable graphitic aqueous bio-interface in large-scale simulations.

Amino acid Adsorption

The free energies of adsorption of the AAs at the aqueous graphene interface calculated from the meta-dynamics simulations are shown in Figure 2. Figure S10 shows the collective variable sampled (the centre of mass of amino acids) as function of time for two representative systems, indicating that the energy landscape has been sampled sufficiently along the reaction coordinate.

The three most strongly adsorbing species were found to be Trp, Tyr and Arg while the weakest binder was Asp. Experimentally, it has been found that peptides that exhibit strong binding affinities to graphitic systems tend to contain a number of aromatic residues.[16] This tallies with our predicted strong binding affinity of Trp, Tyr, and to a lesser extent, Phe. However, it should be noted that comparing the adsorption of single amino acid species with the adsorption data for peptides only allows very indirect comparisons, which must be interpreted with caution. The binding affinity of a peptide is known to not merely comprise the additive sum of the binding affinities of the constituent residues within the peptide, due to the interplay between peptide sequence, conformation and binding affinity.[22,24] Simulations of peptides showing high binding affinities to graphitic systems on graphene[9,16,17,25,32] and/or CNTs[23,29–31] interfaces also indicate the propensity of aromatic residues to adsorb strongly to the graphitic interface.

As with comparisons with experiment, seeking comparisons on an equal footing against existing simulation data can

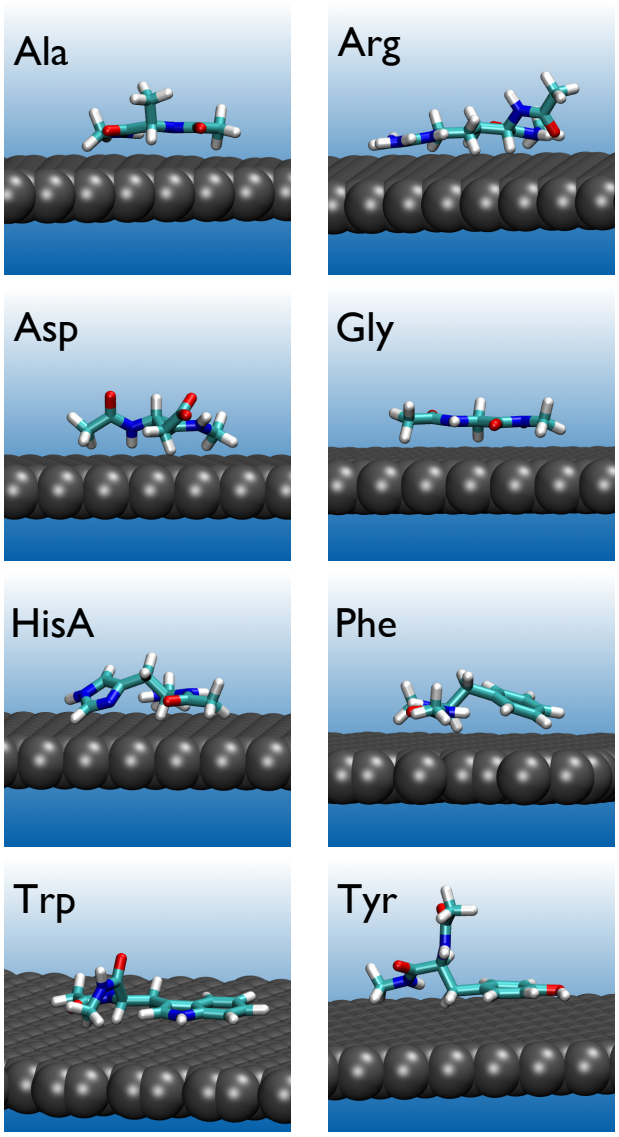

Fig. 3 Snapshots of representative configurations of the adsorbed amino acids from the meta-dynamics simulations. Water not shown for clarity.

also be fraught with challenges. Calculated binding *enthalpies* at aqueous graphene interfaces have been reported for both AAs[25] and residues (in host-guest tri-peptide sequences); no analogous calculated binding *free-energies* have been reported to date.[26] In comparing our findings against these previous works, we note that recent studies have shown that, in some instances (but not all), calculated binding enthalpies on polarisable gold surfaces may differ substantially from their binding free-energy counterparts (even to the point where binding enthalpies can be unfavourable, while the free-energy can show the opposite behaviour).[22,100] As a second complicating factor, neither of these previous studies has employed the same structural model as we have here; we used capped AAs, whilst Pandey *et al.* used zwitterionic AAs, and Camden *et al.* used G-X-G tripeptides in their zwitterionic form. These two caveats, coupled with the fact that each has used a different FF in their simulations, make a detailed, quantitative, and critical evaluation of our findings against those from these past studies impractical.

However, some comments on the chief similarities and differences are warranted. Pandey *et al.* used the AMBER ff99SB FF, and reported the relative binding enthalpy ranking Trp > Tyr > Arg > Phe > HisA > Lys as the strongest binders, and Gly < Ala < Ser as the weakest binders.[25] This ordering of the aromatic species as among the strongest binders broadly tallies with the results of simulations of peptides adsorbing on the surface of graphene/CNTs. Camden *et al.*, using the TEAM FF, reported calculated binding enthalpies for the glycine-residue-extrapolated ΔH_{ads} for the other amino acids.[26] In this study the order of the five residues with the largest ΔH_{ads} was found to be Arg > Gln > Asn > Lys > Gly. Thus, while both these previous studies agree on the strong binding affinity of Arg, they differ considerably in other respects. Camden *et al.* reported much weaker binding affinities for the aromatic residues (Phe was among the five *weakest* binders) than Pandey *et al.* reported for the corresponding AAs, while reporting stronger adsorption of the uncharged polar residues, especially those containing amide groups (Gln and Asn).

In particular, the contrast between the adsorption strength of Gly and Ala amongst these two studies and our work presented here deserves more detailed comment. While Pandey *et al.* reported a ranking in binding enthalpy strength such that Ala > Gly, the opposite was reported for the binding enthalpy strength by Camden *et al.* Our binding free energy trends agree with the trend from Camden *et al.* However, given the apparent discrepancies that can arise between binding enthalpies and free-energies, and the difference in structural models used in all three of these works, we cannot draw any firm conclusions at this time. Nevertheless, we recognise that a trend where the graphene binding strength of Gly is greater than Ala may be, at first sight, counter-intuitive. Certainly, this would be an unexpected and puzzling result if it were found for the gas phase. However, at the *aqueous* interface, the participation of liquid water and the corresponding (and possibly very subtle) contributions to the binding enthalpy and entropy contributions to the binding free energy, arising from the solvent, are more complex.

Moreover, we propose the amide group should have a strong affinity for graphene. This is physically reasonable; it has been determined via our first-principles calculations, such that the GRAPPA FF has implicitly captured the favourable overlap between the partially-delocalised π electron cloud on the

amide group and the delocalised π electron cloud above the graphene surface. We suggest this attraction between the amide and the graphene plays a critical role in the free-energy binding trend between Ala and Gly. Specifically, we found that the amide backbone preferred direct contact with the graphene when adsorbed at the aqueous interface. For Gly, the lack of side-chain atoms (aside from H) ensured that this AA could make very close contact at the aqueous interface. For Ala, we suggest a more subtle competition was taking place, involving the hydrophobic meythl side-chain in Ala. Further analysis of our Ala simulations revealed the distribution of the distance from the methyl carbon to the graphene surface, for instances when the amide backbone was in direct contact with the surface, as shown in the ESI† Figure S11, alongside the interfacial water density, provided for reference. These data show that while a majority of these configurations could position the methyl group in the region of low-density solvent between the first and second layers of interfacial water (which should be a favourable arrangement), the remaining ($\sim$25%) of these configurations exposed the hydrophobic methyl group to a region high water density. We propose this arrangement will be relatively unfavourable, accounting for (in part) the more favourable free energy of adsorption of Gly with respect to Ala.

Snapshots showing representative configurations of the AAs adsorbed at the aqueous graphene interface are provided in Figure 3. The three most strongly adsorbing species, Trp, Tyr and Arg, all primarily, though not solely, adsorbed onto the graphene via their side chains, with the guanidinium group/aromatic-ring lying flat on the surface. In contrast, the aromatic rings of Phe and HisA were often (though not always) tilted rather than lying flat on the surface, with the amide backbone of these AAs maximising their interaction with the graphene interface. As already mentioned, Gly and Ala adsorbed primarily through the amide backbone, which lay parallel to the graphene surface. Asp adsorbed through both the backbone and side-chain and was tilted slightly with respect to the surface.

Figure S12 in the ESI† shows the probability distribution of the angle between the plane of the aromatic ring and the graphene surface when the centre of mass of the AAs were within 9 Å of the graphene surface. It is clear that the rings of Trp and Tyr were alligned more parallel to the graphene surface than Phe and HisA. A similar finding was reported for the aromatic residues within peptides adsorbed onto a CNT, from simulations using AMOEBAPRO.[29] Considering this result in conjunction with the relatively strong binding affinity of Gly, we advance the hypothesis that the tilted configurations of Phe and HisA were due to the relatively weaker adsorption strength of the benzene/imidazole group, giving rise to competition between the aromatic side chain and the amide backbone. In contrast, in the case of Trp and Tyr (and Arg), the interaction of the side-chain with the graphene surface is suggested to be stronger than that of the amide, and consequently this led to the AAs being adsorbed with their side chain lying flat on the surface.

Conclusions

In partnership with experiment, molecular simulation can play a valuable role in enhancing our understanding of how to manipulate the aqueous graphitic bio-interface at the molecular level. Progress in this area has been hindered by the lack of a graphene/water/biomolecule force-field that (1) incorporates polarisation effects, (2) is sufficiently computationally inexpensive to facilitate large, long timescale simulations, and (3) is compatible with a widely-used biomolecule FF. Here, we have developed such a polarisable FF, GRAPPA. In simulations of the graphitic-water interface, GRAPPA largely reproduced results of the high quality, but more expensive AMEOBAPRO and FPMD simulations. Free energies of adsorption were calculated for the aqueous graphene interface, for eight representative amino acids. All eight species showed moderate binding affinities, with Arg, Trp and Tyr showing the strongest binding, primarily via their side chains. Our meta-dyanmics simulations also revealed the strong binding affinity of amide groups at the interface. As an economical, polarisable bio-compatible interfacial force-field that can be readily implemented in mainstream molecular simulation software packages, GRAPPA will aid advances in the biomolecule-mediated manipulation and self-assembly of graphene in aqueous solutions.

Acknowledgements

We thank the Victoria Life Sciences Computational Initiative (VLSCI) and the National Computing Infrastructure (NCI) for provision of computational resources. ZEH and TRW thank **veski** for research funding, and TRW thanks **veski** for an Innovation Fellowship. TRW thanks the EOARD for a Window on Science Award.

References

1 Y. Zhang, T. R. Nayak, H. Hong and W. B. Cai, *Nanoscale*, 2012, **4**, 3833–3842.
2 H. C. Zhang, G. Grüner and Y. L. Zhao, *J. Mater. Chem. B*, 2013, **1**, 2542–2567.
3 Z. Liu, S. M. Tabakman, Z. Chen and H. Dai, *Nat Protoc.*, 2009, **4**, 1372–1381.
4 A. Kalra, S. Garde and G. Hummer, *Proc. Natl. Acad. Sci. USA*, 2003, **100**, 10175–10180.
5 Y. Liu, X. Dong and P. Chen, *Chem. Soc. Rev.*, 2012, **41**, 2283.
6 M. S. Mannoor, H. Tao, J. D. Clayton, A. Sengupta, D. L. Kaplan, R. R. Naik, N. Verma, F. G. Omenetto and M. C. McAlpine, *Nature Comm.*, 2012, **3**, 763.

7 Y. X. Fang and E. K. Wang, *Chem. Commun.*, 2013, **49**, 9526–9539.
8 D. R. Samarajeewa, G. R. Dieckmann, S. O. Nielsen and I. H. Musselman, *Nanoscale*, 2012, **4**, 4544–4554.
9 B. Akdim, R. Pachter, S. S. Kim, R. R. Naik, T. R. Walsh, S. Trohalaki, G. Hong, Z. Kuang and B. L. Farmer, *ACS Appl. Mater. Inter.*, 2013, **5**, 7470–7477.
10 S. Wang, E. S. Humphreys, S.-Y. Chung, D. F. Delduco, S. R. Lustig, H. Wang, K. N. Parker, N. W. Rizzo, S. Subramoney, Y.-M. Chiang and A. Jagota, *Nat. Mater.*, 2003, **2**, 196.
11 Z. Su, T. Leung and J. F. Honek, *J. Phys. Chem. B Lett.*, 2006, 23263.
12 X. Li, W. Chen, Q. Zhan, L. Dai, L. Sowards, M. Pender and R. R. Naik, *J. Phys. Chem. B*, 2006, **110**, 12621–12625.
13 C. G. Salzmann, M. A. H. Ward, R. M. J. Jacobs, G. Tobias and M. L. H. Green, *J. Phys. Chem. C*, 2007, **111**, 18520–18524.
14 H. Xie, E. J. Becraft, R. H. Baughman, A. B. Dalton and G. R. Dieckmann, *J. Peptide Sci.*, 2008, **14**, 139–151.
15 Y. Cui, S. N. Kim, S. E. Jones, L. L. Wissler, R. R. Naik and M. C. McAlpine, *Nano Lett.*, 2010, **10**, 4559–4565.
16 S. N. Kim, Z. Kuang, J. M. Slocik, S. E. Jones, Y. Cui, B. L. Farmer, M. C. McAlpine and R. R. Naik, *J. Am. Chem. Soc.*, 2011, **133**, 14480–14483.
17 J. Katoch, S. N. Kim, Z. Kuang, B. L. Farmer, R. R. Naik, S. A. Tatulian and M. Ishigami, *Nano Lett.*, 2012, **12**, 2342–2346.
18 C. R. So, Y. Hayamizu, H. Yazici, C. Gresswell, D. Khatayevich, C. Tamerler and M. Sarikaya, *ACS Nano*, 2012, **6**, 1648–1656.
19 X. B. Mao, Y. Y. Guo, Y. Luo, L. Niu, L. Liu, X. J. Ma, H. B. Wang, Y. L. Yang, G. H. Wei and C. Wang, *J. Amer. Chem. Soc.*, 2013, **135**, 2181–2187.
20 X. B. Mao, Y. B. Wang, L. Liu, L. Niu, Y. L. Yang and C. Wang, *Langmuir*, 2009, **25**, 8849–8853.
21 Z. Li, T. Uzawa, T. Tanaka, A. Hida, K. Ishibashi, H. Katakura, E. Kobatake and Y. Ito, *Biotechnol. Lett.*, 2013, **35**, 39–45.
22 Z. Tang, J. P. Palafox-Hernandez, W.-C. Law, Z. E. Hughes, M. T. Swihart, P. N. Prasad, M. R. Knecht and T. R. Walsh, *ACS Nano*, 2013, **7**, 9632–9646.
23 S. D. Tomásio and T. R. Walsh, *Mol. Phys.*, 2007, **105**, 221–229.
24 A. A. Skelton, T. N. Liang and T. R. Walsh, *ACS Appl. Mater. Interfaces*, 2009, **1**, 1482–1491.
25 R. B. Pandey, Z. Kuang, B. L. Farmer, S. S. Kim and R. R. Naik, *Soft Matter*, 2012, **8**, 9101.
26 A. N. Camden, S. A. Barr and R. J. Berry, *J. Phys. Chem. B*, 2013, **117**, 10691–10697.
27 T. R. Walsh, *Mol. Phys.*, 2008, **106**, 1613–1619.
28 C. Rajesh, C. Majumder, H. Mizuseki and Y. Kawazoe, *J. Chem. Phys.*, 2009, **130**, 124911.
29 S. M. Tomásio and T. R. Walsh, *J. Phys. Chem. C*, 2009, **113**, 8778–8785.
30 S. R. Friling, R. Notman and T. R. Walsh, *Nanoscale*, 2010, **2**, 98.
31 T. R. Walsh and S. M. Tomasio, *Mol. BioSyst.*, 2010, **6**, 1707–1718.
32 M. Mijajlovic, M. J. Penna and M. J. Biggs, *Langmuir*, 2013, **29**, 2919–2926.
33 J. Schneider and L. Colombi Ciacchi, *J. Amer. Chem. Soc.*, 2012, **134**, 2407–2413.
34 A. Pertsin and M. Grunze, *J. Phys. Chem. B*, 2004, **108**, 1357–1364.
35 R. L. Jaffe, P. Gonnet, T. Werder, J. H. Walther and P. Koumoutsakos, *Mol. Simul.*, 2004, **30**, 205–216.
36 A. Pertsin and M. Grunze, *J. Chem. Phys.*, 2006, **125**, 114707.
37 G. R. Birkett and D. D. Do, *J. Phys. Chem. C*, 2007, **111**, 5735–5742.
38 C. Calero, M. C. Gordillo and J. Martí, *J. Chem. Phys.*, 2013, **138**, 214702.
39 T. A. Ho and A. Striolo, *J. Chem. Phys.*, 2013, **138**, 054117.
40 D. Konatham, J. Yu, T. A. Ho and A. Striolo, *Langmuir*, 2013, **29**, 11884–11897.
41 F. Taherian, V. Marcon and N. F. A. van der Vegt, *Langmuir*, 2013, **29**, 1457–1465.
42 Y. Wu and N. R. Aluru, *J. Phys. Chem. B*, 2013, **117**, 8802–8813.
43 M. C. Gordillo and J. Martí, *J. Phys. Condens. Matter*, 2010, **22**, 284111.
44 A. Alexiadis and S. Kassinos, *Chem. Rev.*, 2008, **108**, 5014– 5034.
45 D. Lu, Y. Li, U. Ravaioli and K. Schulten, *J. Phys. Chem. B*, 2005, **109**, 11461.
46 X. Zhao and J. K. Johnson, *Mol. Simul.*, 2005, **31**, 1–10.
47 F. Moulin, M. Devel and S. Picaud, *Phys. Rev. B*, 2005, **71**, 165401.
48 J. Sala, E. Guardia and J. Martí, *Phys. Chem. Chem. Phys.*, 2012, **14**, 10799.
49 P. Schyman and W. L. Jorgensen, *J. Phys. Chem. Lett.*, 2013, **4**, 468–474.
50 S. D. Chakarova-Käck, E. Schröder, B. I. Lundqvist and D. C. Langreth, *Phys. Rev. Lett.*, 2006, **96**, 146107.
51 E. M. Cabaleiro-Lago, J. A. Carrazana-García and J. Rodríguez-Otero, *J Chem. Phys.*, 2009, **130**, 234307.
52 E. M. Huff and P. Pulay, *Mol. Phys.*, 2009, **107**, 1197–1207.
53 G. R. Jenness and K. D. Jordan, *J. Phys. Chem. C*, 2009, **113**, 10242–10248.
54 M. Rubeš, P. Nachtigall, J. Vondrášek and O. Bludský, *J. Phys. Chem. C*, 2009, **113**, 8412–8419.
55 G. R. Jenness, O. Karalti and K. D. Jordan, *Phys. Chem. Chem. Phys.*, 2010, **12**, 6375.
56 M. Rubeš, J. Kysilka, P. Nachtigall and O. Bludský, *Phys. Chem. Chem. Phys.*, 2010, **12**, 6438–6444.
57 A. Ambrosetti and P. L. Silvestrelli, *J. Phys. Chem. C*, 2011, **115**, 3695–3702.
58 R. R. Q. Freitas, R. Rivelino, F. d. B. Mota and C. M. C. de Castilho, *J. Phys. Chem. A*, 2011, **115**, 12348–12356.
59 J. Ma, A. Michaelides, D. Alfè, L. Schimka, G. Kresse and E. Wang, *Phys. Rev. B*, 2011, **84**, 033402.
60 J. Kysilka, M. Rubeš, L. Grajciar, P. Nachtigall and O. Bludský, *J. Phys. Chem. A*, 2011, **115**, 11387–11393.
61 C. Thierfelder, M. Witte, S. Blankenburg, E. Rauls and W. G. Schmidt, *Surf. Sci.*, 2011, **605**, 746–749.
62 E. Voloshina, D. Usvyat, M. Schütz, Y. Dedkov and B. Paulus, *Phys. Chem. Chem. Phys.*, 2011, **13**, 12041.
63 K. Berland and P. Hyldgaard, *Phys. Rev. B*, 2013, **87**, 205421.
64 P. Lazar, F. Karlický, P. Jurečka, M. Kocman, E. Otyepková, K. Šafářová and M. Otyepka, *J. Am. Chem. Soc.*, 2013, **135**, 6372–6377.
65 J.-H. Lee, Y.-K. Choi, H.-J. Kim, R. H. Scheicher and J.-H. Cho, *J. Phys. Chem. C*, 2013, **117**, 13435–13441.
66 D. G. A. Smith and K. Patkowski, *J. Chem. Theory Comput.*, 2013, **9**, 370–389.
67 T. R. Walsh, *Phys. Chem. Chem. Phys.*, 2005, **7**, 443–451.
68 M. Dion, H. Rydberg, E. Schröder, D. C. Langreth and B. I. Lundqvist, *Phys. Rev. Lett.*, 2004, **92**, 246401.
69 J. Klimeš and A. Michaelides, *J. Chem. Phys.*, 2012, **137**, 120901.
70 P. Tereshchuk and J. L. F. Da Silva, *J. Phys. Chem. C*, 2012, **116**, 24695–24705.
71 L. B. Wright, P. M. Rodger, S. Corni and T. R. Walsh, *J. Chem. Theory Comput.*, 2013, **9**, 1616–1630.
72 J. Carrasco, J. Klimeš and A. Michaelides, *J. Chem. Phys.*, 2013, **138**, 024708.
73 Z. E. Hughes, L. B. Wright and T. R. Walsh, *Langmuir*, 2013, **29**, 13217–13229.
74 L. B. Wright, P. M. Rodger, T. R. Walsh and S. Corni, *J. Phys. Chem. C*, 2013, **117**, 24292–24306.
75 F. Iori and S. Corni, *J. Comput. Chem.*, 2008, **29**, 1656–1666.
76 G. Cicero, J. C. Grossman, E. Schwegler, F. Gygi and G. Galli, *J. Am. Chem. Soc.*, 2008, **130**, 1871–1878.
77 M. K. Rana and A. Chandra, *J. Chem. Phys.*, 2013, **138**, 204702.
78 C. Calero, J. Marti, E. Guardia and M. Masia, *J. Chem. Theory Comput.*,

2013, **9**, 5070–5075.
79 P. Ren and J. W. Ponder, *J. Comput. Chem.*, 2002, **23**, 1497–1506.
80 J. W. Ponder and D. A. Case, *Adv. Protein Chem.*, 2003, **66**, 27–85.
81 P. Ren and J. W. Ponder, *J. Phys. Chem. B*, 2003, **107**, 5933–5947.
82 A. Barducci, G. Bussi and M. Parrinello, *Phys. Rev. Lett.*, 2008, **100**, 020603.
83 P. Giannozzi, S. Baroni, N. Bonini, M. Calandra, R. Car, C. Cavazzoni, D. Ceresoli, G. L. Chiarotti, M. Cococcioni, I. Dabo, A. D. Corso, S. de Gironcoli, S. Fabris, G. Fratesi, R. Gebauer, U. Gerstmann, C. Gougoussis, A. Kokalj, M. Lazzeri, L. Martin-Samos, N. Marzari, F. Mauri, R. Mazzarello, S. Paolini, A. Pasquarello, L. Paulatto, C. Sbraccia, S. Scandolo, G. Sclauzero, A. P. Seitsonen, A. Smogunov, P. Umari and R. M. Wentzcovitch, *J. Phys. Condens. Matter*, 2009, **21**, 395502.
84 D. Vanderbilt, *Phys. Rev. B*, 1990, **41**, 7892.
85 É. D. Murray, K. Lee and D. C. Langreth, *J. Chem. Theory Comput.*, 2009, **5**, 2754–2762.
86 K. Lee, É. D. Murray, L. Kong, B. I. Lundqvist and D. C. Langreth, *Phys. Rev. B*, 2010, **82**, 081101.
87 J. Klimeš, D. R. Bowler and A. Michaelides, *J. Phys.: Condens. Matter*, 2010, **22**, 022201.
88 V. R. Cooper, *Phys. Rev. B*, 2010, **81**, 161104.
89 A. D. MacKerell, Jr, D. Bashford, M. Bellott, R. L. Dunbrack, Jr, J. D. Evanseck, M. J. Field, S. Fischer, J. Gao, H. Guo and S. Ha, *J. Phys. Chem. B*, 1998, **102**, 3586–3616.
90 S. Piana, K. Lindorff-Larsen and D. E. Shaw, *Biophys. J.*, 2011, **100**, L47–L49.
91 B. Hess, C. Kutzner, D. Van Der Spoel and E. Lindahl, *J. Chem. Theory Comput.*, 2008, **4**, 435–447.
92 M. Bonomi, D. Branduardi, G. Bussi, C. Camilloni, D. Provasi, P. Raiteri, D. Donadio, F. Marinelli, F. Pietrucci and R. A. Broglia, *Comput. Phys. Comm.*, 2009, **180**, 1961–1972.
93 W. L. Jorgensen, J. Chandrasekhar, J. D. Madura, R. W. Impey and M. L. Klein, *J. Chem. Phys.*, 1983, **79**, 926–935.
94 E. Neria, S. Fischer and M. Karplus, *J. Phys. Chem.*, 1996, **105**, 1029–1921.
95 W. Hoover, *Phys. Rev. A*, 1985, **31**, 1695–1697.
96 R. Zacharia, H. Ulbricht and T. Hertel, *Phys. Rev. B*, 2004, **69**, 155406.
97 J. W. Ponder, P. Ren, R. V. Pappu, R. K. Hart, M. E. Hodgson, D. P. Cistola, C. E. Kundrot and F. M. Richards, *Software tools for molecular design*, Washington Universtiy School of Medicine, 4th edn., 2004.
98 A. J. Stone, *Chem. Phys. Lett.*, 1981, **83**, 233–239.
99 A. J. Stone and M. Alderton, *Mol. Phys.*, 1985, **56**, 1047–1064.
100 M. Rosa, S. Corni and R. Di Felice, *J. Chem. Theory Comput.*, 2014, in press, **dx.doi.org/10.1021/ct401117g**